

Two-Dimensional Pulsar Distance Inference from Nanohertz Gravitational Waves

Si-Ren Xiao,¹ Ji-Yu Song,¹ Yue Shao,² Ling-Feng Wang,³ Jing-Fei Zhang,¹ and Xin Zhang^{1, 4, 5, *}

¹*Liaoning Key Laboratory of Cosmology and Astrophysics,*

College of Sciences, Northeastern University, Shenyang 110819, China

²*Department of Physics, Liaoning Normal University, Dalian 116029, China*

³*School of Physics and Optoelectronic Engineering, Hainan University, Haikou 570228, China*

⁴*MOE Key Laboratory of Data Analytics and Optimization for Smart Industry,*

Northeastern University, Shenyang 110819, China

⁵*National Frontiers Science Center for Industrial Intelligence and Systems Optimization,*
Northeastern University, Shenyang 110819, China

Pulsar timing arrays (PTAs) are limited in localizing nanohertz continuous gravitational waves (CGWs) by uncertainties in pulsar distances. We introduce a method to infer pulsar distances in two dimensions, using phase information from the pulsar terms of multiple CGW sources. Our approach can enhance distance precision and, in some cases, achieve order-of-magnitude improvements relative to existing one-dimensional distance-inference methods. Using simulations of an SKA-era PTA with realistic parallax-based distance priors, we demonstrate that pulsars at ~ 1 kpc can achieve sub-parsec distance precision with only a few CGW sources. Such improvements in pulsar-distance precision have important implications for CGW host-galaxy identification and multimessenger observational prospects.

Introduction.—Nanohertz gravitational waves (GWs) can be detected with pulsar timing arrays (PTAs), which track pulse times of arrival from ensembles of exceptionally stable millisecond pulsars. Passing GWs perturb the Earth-pulsar light-travel time, imprinting characteristic signatures in the timing residuals.

Several PTA collaborations have recently reported evidence for a stochastic gravitational-wave background (SGWB) [1–5]. The SGWB may arise from various astrophysical and cosmological sources [6–9], with the leading astrophysical contribution expected from the collective GW emission of supermassive black hole binaries (SMBHBs).

In addition to the SGWB, continuous gravitational waves (CGWs) from individual SMBHBs are an equally important PTA target [10–14]. Identifying their host galaxies, and possibly electromagnetic counterparts, would enable powerful multimessenger studies, such as using nanohertz CGWs to measure the Hubble constant [15–19] through standard-siren methods [20–25]. However, PTAs are expected to localize CGW sources only to $\sim 10^2\text{--}10^3 \text{ deg}^2$ [26–30], limiting host-galaxy identification. This poor localization arises mainly from large uncertainties in pulsar distances, which severely limit the contribution of the pulsar term and lead most studies to treat it as an additional source of self-noise [31–33]. Notably, if pulsar distances can be measured with uncertainties below the GW wavelength (about 1 pc at 10 nHz), the pulsar terms can be effectively exploited in the analysis, leading to significantly improved sky localization of CGW sources [34–38].

In current PTAs, pulsar-distance uncertainties typically range from tens to hundreds of parsecs, with only

a small number of nearby pulsars measured to parsec-level precision through timing or Very Long Baseline Interferometry parallax and kinematic methods [39–41]. Future radio facilities, such as the Square Kilometre Array (SKA), are expected to improve parallax precision [36, 42]. However, parallax precision degrades rapidly with distance, and most PTA pulsars lie at kiloparsec scales where achieving sub-parsec distance precision is challenging. These considerations motivate the exploration of additional approaches to constraining pulsar distances.

CGWs provide a complementary means of measuring pulsar distances through the phase difference between the Earth and pulsar terms. For a single CGW source, the phase difference between the Earth term and the pulsar term is measured only modulo 2π , producing a periodic distance degeneracy that prevents precise pulsar-distance inference. Lee et al. [36] showed that combining the CGW phase information with a precise parallax prior can break this periodicity, but this method is effective only for relatively nearby pulsars with tight parallax constraints. More recently, McGrath et al. [43] and Yu and Pan [44] showed that multiple CGW sources can constrain pulsar distances. This arises because each source's GW parameters produce distinct periodic structures in pulsar distance posteriors, and mismatched periodicities can suppress the spurious modes in the joint posterior, potentially yielding a dominant peak at the pulsar's true distance.

Developing practical pulsar-distance inference methods with multiple CGW sources remains challenging. In principle, a fully joint analysis across all pulsars is statistically optimal, but it becomes computationally intractable for realistic datasets, as the multimodal distance posteriors of many pulsars lead to an exponentially growing parameter space. Existing studies rely on the one-dimensional, single-pulsar distance posteriors to in-

* Corresponding author; zhangxin@neu.edu.cn

fer pulsar distances when combining information from multiple GW sources. However, in single-pulsar analyses, the multimodal structure of the distance posterior is often suppressed by degeneracies between distance and parameters such as the chirp mass and the initial GW frequency, thereby limiting the ability of GW observations to constrain pulsar distances.

In this work, we develop a two-dimensional joint-posterior method for pulsar-distance inference using multiple CGW sources, which explicitly recovers the multimodal distance information lost in single-pulsar analyses due to distance-parameter degeneracies. Our method attains sub-parsec pulsar-distance precision while requiring significantly fewer GW sources than existing one-dimensional approaches, demonstrating the feasibility of high-precision pulsar-distance measurements with multiple CGW sources.

Simulations and distance inference.—CGWs from a circular, GW-driven SMBHB induce timing residuals of the form $s(t, \hat{\Omega}) = F^+(\hat{\Omega}) \Delta s_+(t) + F^\times(\hat{\Omega}) \Delta s_\times(t)$, where $\hat{\Omega}$ is the GW propagation direction and $F^{+,\times}(\hat{\Omega})$ are the standard PTA antenna-pattern functions. The quantities $\Delta s_{+,\times}(t)$ represent the difference between the Earth and pulsar terms,

$$\Delta s_{+,\times}(t) = s_{+,\times}(t) - s_{+,\times}(t_p), \quad (1)$$

where $t_p = t - L_p(1 + \hat{\Omega} \cdot \hat{p})$ is the time at which the pulsar term is evaluated, L_p is the pulsar distance, and \hat{p} is the unit vector from the Earth to the pulsar. Because the pulsar-term phase depends on L_p only modulo 2π , the CGW source generates a series of distance-degenerate modes, producing an intrinsically multi-peak likelihood. Explicit waveform expressions are adopted from Refs. [37, 45, 46].

In our analysis, we assume that the sky locations of the CGW sources used for pulsar-distance inference are known and therefore treat their polar and azimuthal angles as fixed parameters. This does not rely on precise PTA localization as an input to our method. Such sky positions can be provided either by targeted CGW searches toward SMBHB candidates suggested by electromagnetic observations, where a detection confirms the association with the host galaxy [45, 47], or by all-sky CGW searches followed by host-galaxy filtering and ranking within the PTA credible sky region, which can in favorable cases reduce the candidates to a single host [27, 28, 30, 48, 49]. Our method applies whenever a small number of CGW sources have externally determined sky positions.

Following Ref. [37], we construct an SKA-era PTA using the sky positions of 85 pulsars drawn from current PTA datasets. Published distance estimates from the latest PTA releases [50, 51] and the Australia Telescope National Facility Pulsar Catalogue [52] are adopted as fiducial values. We assume an observing timespan of 20 yr and a uniform cadence of 2 weeks. Motivated by SKA forecasts indicating sub-100-ns timing precision [53], we

model the timing noise as white Gaussian noise with $\sigma_n = 50$ ns or 100 ns.

We simulate a catalog of detectable CGW sources following the PTA-detectable population model of Ref. [54], in which sources cluster around a chirp mass of $\mathcal{M} \sim 5 \times 10^9 M_\odot$ and frequencies in the range 3–15 nHz. We fix the chirp mass to $\mathcal{M} = 5 \times 10^9 M_\odot$ and draw source frequencies from the model distribution. We generate 100 SMBHBs isotropically over the sky and adopt a fiducial luminosity distance of $d_L = 1$ Gpc, representative of loud PTA-detectable CGW sources.

For each configuration with $N = 2, 3, 4$, and 5 detectable sources, we perform 1000 realizations by randomly sampling N sources from the catalog and carrying out pulsar-distance inference for each realization.

We perform Bayesian inference on the simulated PTA data using the standard Gaussian likelihood for timing residuals, adopting the same priors for the free parameters as in Ref. [37]. The posterior is sampled with an ensemble MCMC method. The timing model for each CGW source depends on eight source parameters $(\theta, \phi, \log d_L, \iota, \mathcal{M}, \psi, \Phi_0, f_0)$, together with the pulsar distance L_p of each pulsar. Here (θ, ϕ) denote the sky location of the source, d_L is the luminosity distance, ι is the inclination angle, \mathcal{M} is the chirp mass, ψ is the polarization angle, Φ_0 is the initial GW phase, and f_0 is the initial GW frequency. Although the pulsar-term initial phases $\{\Phi_p\}$ are not independent parameters, we sample them as free parameters to avoid the highly oscillatory likelihood structure that makes direct sampling in L_p inefficient [55]. Notably, for each pulsar distance we impose Gaussian priors with a standard deviation σ_p determined by the forecasted SKA-era timing-parallax precision, typically $\mathcal{O}(10\text{ pc})$ for pulsars at ~ 1 kpc, depending on the timing noise and geometry [36].

Given the sampled posterior of the GW parameters, we further extract the pulsar-distance information encoded in Φ_p by using the analytic pulsar-term initial phase-distance relation. Additional details of this relation are provided in the Supplementary Material. Because Φ_p is defined only modulo 2π , the mapping yields multiple distance solutions for each posterior sample, producing a sequence of k -indexed peaks in the resulting distance distribution.

Previous one-dimensional approaches attempted to suppress the spurious k -peaks by multiplying the distance posteriors from multiple CGW sources for a single pulsar [44]. Different sources impose distinct periodicities on L_p , so their posterior product can enhance the true peak. In practice the uncertainties in the GW parameters often wash out the periodicity of these one-dimensional posteriors, limiting the ability of this method to measure the pulsar distance.

We construct a two-dimensional distance posterior for each pulsar pair (p, q) , using all N CGW sources,

$$\text{PDF}_{pq}(L_p, L_q) \propto \pi_{pq}(L_p, L_q) \prod_{n=1}^N \mathcal{P}_{\Phi_{pq},n}(L_p, L_q). \quad (2)$$

Here $\pi_{pq}(L_p, L_q)$ is the joint prior for the pulsar distances, and $\mathcal{P}_{\Phi_{pq},n}(L_p, L_q)$ represents the contribution of the n -th CGW source, obtained by mapping pulsar-term phase posteriors of pulsars p and q into (L_p, L_q) . We neglect the pulsar-distance information carried by the frequency differences between the Earth term and the pulsar terms, as the resulting distance constraints are negligible relative to the pulsar-distance prior. Marginalizing over L_q yields a one-dimensional posterior for pulsar p ,

$$\text{PDF}_p^{(q)}(L_p) = \int dL_q \text{PDF}_{pq}(L_p, L_q). \quad (3)$$

Repeating this for all $q \neq p$ produces a set of posteriors $\{\text{PDF}_p^{(q)}\}$. We adopt the one with the smallest half-width of the 68% credible interval as the final constraint for pulsar p , as this choice maximizes the retained information on L_p among all such two-dimensional constructions. We define this half-width as the pulsar-distance uncertainty and denote it by ΔL_p .

Pulsar distance constraints from CGWs.—For individual GW sources, the two-dimensional posterior distributions for pulsar distances consist of periodic, approximately parallel degeneracy bands. An illustrative example is shown in Fig. 1, which displays the posteriors for the distances to pulsars J0030+0451 and J0613-0200 from three representative GW sources in our simulated catalog, as well as their combined constraint. The spacing of these bands is primarily set by the GW source-pulsar angles α_p and the GW frequency, and therefore differs among sources. When pulsar distance posteriors from multiple GW sources are combined, mismatched bands are suppressed, and the posteriors remain mutually consistent only near the true pulsar distances, yielding a precise pulsar distance measurement. The origin of degeneracies between pulsar distances is discussed in the Supplemental Material.

For comparison, the dashed lines in the one-dimensional marginal panels show the results obtained with the existing method, which infers the pulsar distances from one-dimensional marginalized posteriors. This one-dimensional marginalization inevitably projects the distance-distance degeneracies onto a single axis, significantly washing out the multi-peak structure. Consequently, one-dimensional combinations of multiple GW sources are less effective at isolating the true peak in the pulsar distance than two-dimensional combinations. In this case, the distance to J0613-0200 has a half-width of 0.4 pc for the 68% credible interval from the two-dimensional posterior, substantially smaller than the 6.5 pc obtained with the one-dimensional analysis. Although these results are based on an illustrative example, the statistical performance of our method is evaluated in the following paragraph.

Figure 2 presents the violin-plot distributions of the pulsar-distance uncertainty ΔL_p , obtained from 1000 independent realizations with a 20-year observation time span, for the representative pulsar J0613-0200 at a distance of 0.99 kpc. For a timing-noise level of $\sigma_n = 50$ ns,

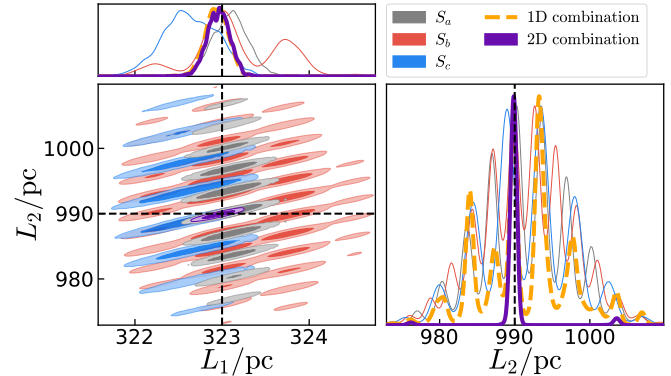


FIG. 1. Example of pulsar distance inference from the joint two-dimensional posterior obtained by combining three GW sources. Posterior distributions of the distances of pulsars J0030+0451 and J0613-0200 (L_1, L_2), including individual posteriors from the three sources and their combined joint posterior (2D combination). For comparison, we also show the result obtained with the method of Ref. [44], which combines the one-dimensional posteriors for each pulsar distance (1D combination). The 1D combination results are shown in orange in the diagonal subplots. Black dashed lines indicate the injected true distances.

four GW sources yield sub-parsec precision in about 90% of the realizations, whereas five sources further tighten the constraint. At $\sigma_n = 100$ ns, sub-parsec precision is obtained in roughly half of the realizations when five GW sources are available. Overall, the distance precision is highly sensitive to both the number of available GW sources and the overall timing-noise level. In particular, for $N = 5$, the inferred distance uncertainties

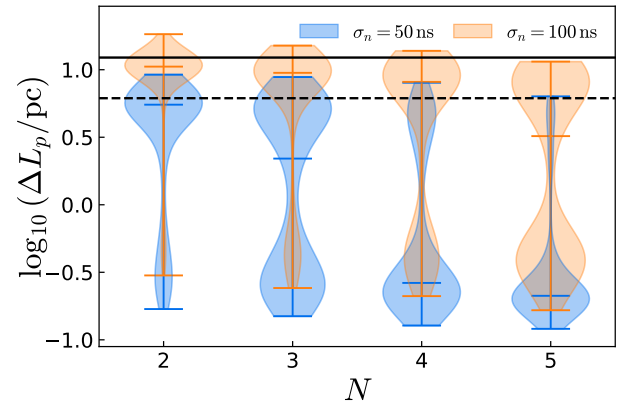


FIG. 2. Distributions of the pulsar-distance uncertainty ΔL_p inferred using different numbers N of GW sources, based on 1000 independent realizations. Shown for a representative pulsar at 0.99 kpc (J0613-0200). Blue and orange violins correspond to timing-noise levels of $\sigma_n = 50$ ns and 100 ns, respectively. Dashed and solid horizontal lines indicate the timing-parallax prior uncertainties σ_{L_p} corresponding to $\sigma_n = 50$ ns and 100 ns.

fall well below the timing-parallax prior σ_{L_p} , demonstrating that combining electromagnetic distance constraints with GW observations can significantly improve pulsar distance measurements. The width of the violin distributions reflects the scatter across realizations arising from source parameters such as sky location and frequency randomly drawn from their underlying distributions.

Results for nearer and more distant pulsars, as well as a comparison between two-dimensional joint-posterior and one-dimensional single-pulsar distance inference, are shown in the Supplemental Material. A full joint inference among more pulsar distances would in principle retain additional information, but exploring such higher-dimensional combinations would substantially increase the complexity of the inference. In this work, we focus on the two-dimensional joint posterior as the minimal extension beyond one dimension that captures the distance-distance degeneracy between two pulsars.

Conclusions.—We have demonstrated that nanohertz CGWs can be used to measure pulsar distances. Building on previous work, we introduce a method that combines two-dimensional pulsar-distance posteriors inferred from multiple GW signals. By mitigating the influence of GW parameter uncertainties on pulsar-distance inference and avoiding the prohibitive computational cost of a joint inference over all pulsar-distance parameters in the PTA, our approach enables robust pulsar-distance measurements based on pulsar-term signals.

Applying our method to a simulated SKA-era PTA, we find that only a small number of CGW sources are required to achieve sub-parsec precision in pulsar-distance measurements when combined with realistic prior distance information from electromagnetic observations. Our analysis is performed in a simplified PTA setting that includes a CGW signal in white noise. Quantifying the impact of additional GW signals, such as overlapping CGW sources and SGWB, as well as additional noise processes, on pulsar-distance inference is a natural and necessary extension of this work.

Achieving sub-parsec precision in pulsar-distance measurements enables more effective use of GW pulsar-term signals, leading to tighter localization of poorly localized GW sources and thereby facilitating SMBHB host-galaxy identification. This capability substantially enhances the prospects for multimessenger astronomy and supports future applications in cosmology and fundamental-physics studies with nanohertz GWs.

Acknowledgments.—We thank Ji-Guo Zhang and Tian-Nuo Li for helpful discussions. This work was supported by the National Natural Science Foundation of China (Grants Nos. 12473001, 12575049, 12533001, and 12305058), the National SKA Program of China (Grants Nos. 2022SKA0110200 and 2022SKA0110203), the China Manned Space Program (Grant No. CMS-CSST-2025-A02), the 111 Project (Grant No. B16009), and the Natural Science Foundation of Hainan Province (Grant No. 424QN215).

[1] G. Agazie *et al.* (NANOGrav), The NANOGrav 15 yr Data Set: Evidence for a Gravitational-wave Background, *Astrophys. J. Lett.* **951**, L8 (2023), [arXiv:2306.16213 \[astro-ph.HE\]](https://arxiv.org/abs/2306.16213).

[2] J. Antoniadis *et al.* (EPTA), The second data release from the European Pulsar Timing Array III. Search for gravitational wave signals, *Astron. Astrophys.* **678**, A50 (2023), [arXiv:2306.16214 \[astro-ph.HE\]](https://arxiv.org/abs/2306.16214).

[3] D. J. Reardon *et al.*, Search for an Isotropic Gravitational-wave Background with the Parkes Pulsar Timing Array, *Astrophys. J. Lett.* **951**, L6 (2023), [arXiv:2306.16215 \[astro-ph.HE\]](https://arxiv.org/abs/2306.16215).

[4] H. Xu *et al.*, Searching for the Nano-Hertz Stochastic Gravitational Wave Background with the Chinese Pulsar Timing Array Data Release I, *Res. Astron. Astrophys.* **23**, 075024 (2023), [arXiv:2306.16216 \[astro-ph.HE\]](https://arxiv.org/abs/2306.16216).

[5] M. T. Miles *et al.*, The MeerKAT Pulsar Timing Array: first data release, *Mon. Not. Roy. Astron. Soc.* **519**, 3976 (2023), [arXiv:2212.04648 \[astro-ph.HE\]](https://arxiv.org/abs/2212.04648).

[6] X. Siemens, V. Mandic, and J. Creighton, Gravitational wave stochastic background from cosmic (super)strings, *Phys. Rev. Lett.* **98**, 111101 (2007), [arXiv:astro-ph/0610920](https://arxiv.org/abs/astro-ph/0610920).

[7] P. Schwaller, Gravitational Waves from a Dark Phase Transition, *Phys. Rev. Lett.* **115**, 181101 (2015), [arXiv:1504.07263 \[hep-ph\]](https://arxiv.org/abs/1504.07263).

[8] R.-G. Cai, Z.-K. Guo, J. Liu, L. Liu, and X.-Y. Yang, Primordial black holes and gravitational waves from para-

metric amplification of curvature perturbations, *JCAP* **06**, 013, [arXiv:1912.10437 \[astro-ph.CO\]](https://arxiv.org/abs/1912.10437).

[9] J. Ellis and M. Lewicki, Cosmic String Interpretation of NANOGrav Pulsar Timing Data, *Phys. Rev. Lett.* **126**, 041304 (2021), [arXiv:2009.06555 \[astro-ph.CO\]](https://arxiv.org/abs/2009.06555).

[10] A. Sesana, A. Vecchio, and M. Volonteri, Gravitational waves from resolvable massive black hole binary systems and observations with Pulsar Timing Arrays, *Mon. Not. Roy. Astron. Soc.* **394**, 2255 (2009), [arXiv:0809.3412 \[astro-ph\]](https://arxiv.org/abs/0809.3412).

[11] S. Babak and A. Sesana, Resolving multiple supermassive black hole binaries with pulsar timing arrays, *Phys. Rev. D* **85**, 044034 (2012), [arXiv:1112.1075 \[astro-ph.CO\]](https://arxiv.org/abs/1112.1075).

[12] X.-J. Zhu, L. Wen, G. Hobbs, Y. Zhang, Y. Wang, D. R. Madison, R. N. Manchester, M. Kerr, P. A. Rosado, and J.-B. Wang, Detection and localization of single-source gravitational waves with pulsar timing arrays, *Mon. Not. Roy. Astron. Soc.* **449**, 1650 (2015), [arXiv:1502.06001 \[astro-ph.IM\]](https://arxiv.org/abs/1502.06001).

[13] Y. Wang and S. D. Mohanty, Pulsar Timing Array Based Search for Supermassive Black Hole Binaries in the Square Kilometer Array Era, *Phys. Rev. Lett.* **118**, 151104 (2017), [Erratum: *Phys. Rev. Lett.* 124, 169901 (2020)], [arXiv:1611.09440 \[astro-ph.IM\]](https://arxiv.org/abs/1611.09440).

[14] C. M. F. Mingarelli, T. J. W. Lazio, A. Sesana, J. E. Greene, J. A. Ellis, C.-P. Ma, S. Croft, S. Burke-Spolaor, and S. R. Taylor, The Local Nanohertz Gravitational-Wave Landscape From Supermassive Black Hole Bina-

ries, *Nature Astron.* **1**, 886 (2017), arXiv:1708.03491 [astro-ph.GA].

[15] D. L. Jow and U.-L. Pen, Measuring Cosmic Expansion with Diffractive Gravitational Scintillation of Nanohertz Gravitational Waves, *Phys. Rev. Lett.* **134**, 131001 (2025), arXiv:2407.03214 [astro-ph.CO].

[16] C. Yan, W. Zhao, and Y. Lu, On Using Inspiring Supermassive Binary Black Holes in the PTA Frequency Band as Standard Sirens to Constrain Dark Energy, *Astrophys. J.* **889**, 10 (2020), arXiv:1912.04103 [astro-ph.CO].

[17] L.-F. Wang, Y. Shao, S.-R. Xiao, J.-F. Zhang, and X. Zhang, Ultra-low-frequency gravitational waves from individual supermassive black hole binaries as standard sirens, *JCAP* **05**, 095, arXiv:2201.00607 [astro-ph.CO].

[18] S.-J. Jin, S.-S. Xing, Y. Shao, J.-F. Zhang, and X. Zhang, Joint constraints on cosmological parameters using future multi-band gravitational wave standard siren observations*, *Chin. Phys. C* **47**, 065104 (2023), arXiv:2301.06722 [astro-ph.CO].

[19] S.-J. Jin, J.-Y. Song, T.-Y. Sun, S.-R. Xiao, H. Wang, L.-F. Wang, J.-F. Zhang, and X. Zhang, Gravitational wave standard sirens: A brief review of cosmological parameter estimation, *Sci. China Phys. Mech. Astron.* **69**, 220401 (2026), arXiv:2507.12965 [astro-ph.CO].

[20] B. F. Schutz, Determining the Hubble Constant from Gravitational Wave Observations, *Nature* **323**, 310 (1986).

[21] S.-J. Jin, Y.-Z. Zhang, J.-Y. Song, J.-F. Zhang, and X. Zhang, Taiji-TianQin-LISA network: Precisely measuring the Hubble constant using both bright and dark sirens, *Sci. China Phys. Mech. Astron.* **67**, 220412 (2024), arXiv:2305.19714 [astro-ph.CO].

[22] J.-Y. Song, L.-F. Wang, Y. Li, Z.-W. Zhao, J.-F. Zhang, W. Zhao, and X. Zhang, Synergy between CSST galaxy survey and gravitational-wave observation: Inferring the Hubble constant from dark standard sirens, *Sci. China Phys. Mech. Astron.* **67**, 230411 (2024), arXiv:2212.00531 [astro-ph.CO].

[23] J.-Y. Song, J.-Z. Qi, J.-F. Zhang, and X. Zhang, Model-independent H_0 within FLRW: Joint Constraints from GWTC-3 Standard Sirens and Strong Lensing Time Delays, *Astrophys. J. Lett.* **985**, L44 (2025), arXiv:2503.10346 [astro-ph.CO].

[24] A. G. Abac *et al.* (LIGO Scientific, VIRGO, KAGRA), GWTC-4.0: Constraints on the Cosmic Expansion Rate and Modified Gravitational-wave Propagation, (2025), arXiv:2509.04348 [astro-ph.CO].

[25] J.-Y. Song, G.-H. Du, T.-N. Li, L.-F. Wang, J.-Z. Qi, J.-F. Zhang, and X. Zhang, Gravitational wave standard sirens from GWTC-3 combined with DESI DR2 and DESY5: A late-universe probe of the Hubble constant and dark energy, (2025), arXiv:2511.12017 [astro-ph.CO].

[26] S. R. Taylor, E. A. Huerta, J. R. Gair, and S. T. McWilliams, Detecting eccentric supermassive black hole binaries with pulsar timing arrays: Resolvable source strategies, *Astrophys. J.* **817**, 70 (2016), arXiv:1505.06208 [gr-qc].

[27] J. M. Goldstein, A. Sesana, A. M. Holgado, and J. Veitch, Associating host galaxy candidates to massive black hole binaries resolved by pulsar timing arrays, *Mon. Not. Roy. Astron. Soc.* **485**, 248 (2019), arXiv:1812.02670 [astro-ph.IM].

[28] P. Petrov, S. R. Taylor, M. Charisi, and C.-P. Ma, Identifying the Host Galaxies of Supermassive Black Hole Binaries Found by Pulsar Timing Arrays, *Astrophys. J.* **976**, 129 (2024), arXiv:2406.04409 [astro-ph.GA].

[29] S.-R. Xiao, Y. Shao, L.-F. Wang, J.-Y. Song, L. Feng, J.-F. Zhang, and X. Zhang, Nanohertz gravitational waves from a quasar-based supermassive black hole binary population model as dark sirens, *JCAP* **04**, 060, arXiv:2408.00609 [astro-ph.CO].

[30] R. J. Truant, D. Izquierdo-Villalba, A. Sesana, G. M. Shaifullah, M. Bonetti, D. Spinoso, and S. Bonoli, Lighting up the nano-hertz gravitational wave sky: opportunities and challenges of multimessenger astronomy with PTA experiments, (2025), arXiv:2504.01074 [astro-ph.GA].

[31] S. Taylor, J. Ellis, and J. Gair, Accelerated Bayesian model-selection and parameter-estimation in continuous gravitational-wave searches with pulsar-timing arrays, *Phys. Rev. D* **90**, 104028 (2014), arXiv:1406.5224 [gr-qc].

[32] M. Charisi, S. R. Taylor, C. A. Witt, and J. Runnoe, Efficient Large-Scale, Targeted Gravitational-Wave Probes of Supermassive Black-Hole Binaries, *Phys. Rev. Lett.* **132**, 061401 (2024), arXiv:2304.03786 [gr-qc].

[33] K. Grunthal, N. Porayko, D. J. Champion, and M. Kramer, The role of distant pulsars in the detectability of continuous gravitational waves, (2025), arXiv:2512.04589 [astro-ph.HE].

[34] L. Boyle and U.-L. Pen, Pulsar timing arrays as imaging gravitational wave telescopes: angular resolution and source (de)confusion, *Phys. Rev. D* **86**, 124028 (2012), arXiv:1010.4337 [astro-ph.HE].

[35] V. Corbin and N. J. Cornish, Pulsar Timing Array Observations of Massive Black Hole Binaries, arXiv e-prints (2010), arXiv:1008.1782 [astro-ph.HE].

[36] K. J. Lee *et al.*, Gravitational wave astronomy of single sources with a pulsar timing array, *Mon. Not. Roy. Astron. Soc.* **414**, 3251 (2011), arXiv:1103.0115 [astro-ph.HE].

[37] R. Kato and K. Takahashi, Realistic assessment of a single gravitational wave source localization taking into account precise pulsar distances with pulsar timing arrays, *Phys. Rev. D* **113**, 022001 (2026), arXiv:2506.02819 [gr-qc].

[38] A. C. Tsai, D. L. Jow, and U.-L. Pen, Reaching diffraction-limited localization with coherent ptas, (2025), arXiv:2512.10795 [astro-ph.IM].

[39] A. T. Deller *et al.*, Microarcsecond VLBI Pulsar Astrometry with PSR π II. Parallax Distances for 57 Pulsars, *Astrophys. J.* **875**, 100 (2019), arXiv:1808.09046 [astro-ph.IM].

[40] H. Ding *et al.*, The MSPSR π catalogue: VLBA astrometry of 18 millisecond pulsars, *Mon. Not. Roy. Astron. Soc.* **519**, 4982 (2023), arXiv:2212.06351 [astro-ph.HE].

[41] D. J. Reardon *et al.*, The Neutron Star Mass, Distance, and Inclination from Precision Timing of the Brilliant Millisecond Pulsar J0437-4715, *Astrophys. J. Lett.* **971**, L18 (2024), arXiv:2407.07132 [astro-ph.HE].

[42] R. Smits, S. J. Tingay, N. Wex, M. Kramer, and B. Stappers, Prospects for accurate distance measurements of pulsars with the SKA: enabling fundamental physics, *Astron. Astrophys.* **528**, A108 (2011), arXiv:1101.5971 [astro-ph.IM].

[43] C. McGrath, D. J. D’Orazio, and J. Creighton, Measuring the Hubble constant with double gravitational wave sources in pulsar timing, *Mon. Not. Roy. Astron. Soc.*

517, 1242 (2022), arXiv:2208.06495 [astro-ph.CO].

[44] J. Yu and Z. Pan, Subparsec precision measurement of pulsar distances with nanohertz gravitational waves, *Phys. Rev. D* **112**, 023012 (2025), arXiv:2503.23017 [astro-ph.HE].

[45] N. Agarwal *et al.*, The NANOGrav 15 yr Data Set: Targeted Searches for Supermassive Black Hole Binaries, (2025), arXiv:2508.16534 [astro-ph.HE].

[46] B. Bécsy, N. J. Cornish, and M. C. Digman, Fast Bayesian analysis of individual binaries in pulsar timing array data, *Phys. Rev. D* **105**, 122003 (2022), arXiv:2204.07160 [gr-qc].

[47] L.-W. Tian, Y.-C. Bi, Y.-M. Wu, and Q.-G. Huang, Targeted search for an individual SMBHB in NANOGrav 15-year and EPTA DR2 data sets, (2025), arXiv:2508.14742 [astro-ph.GA].

[48] J. Bardati, J. J. Ruan, D. Haggard, and M. Tremmel, Signatures of Massive Black Hole Merger Host Galaxies from Cosmological Simulations. I. Unique Galaxy Morphologies in Imaging, *Astrophys. J.* **961**, 34 (2024), arXiv:2308.03828 [astro-ph.GA].

[49] P. Horlaville, J. J. Ruan, M. Eracleous, J. Bardati, J. C. Runnoe, and D. Haggard, Predicting Potential Host Galaxies of Supermassive Black Hole Binaries Based on Stellar Kinematics in Archival IFU Surveys, (2025), arXiv:2504.21145 [astro-ph.GA].

[50] G. Agazie *et al.* (NANOGrav), The NANOGrav 15 yr Data Set: Bayesian Limits on Gravitational Waves from Individual Supermassive Black Hole Binaries, *Astrophys. J. Lett.* **951**, L50 (2023), arXiv:2306.16222 [astro-ph.HE].

[51] J. Antoniadis *et al.* (EPTA), The second data release from the European Pulsar Timing Array - I. The dataset and timing analysis, *Astron. Astrophys.* **678**, A48 (2023), arXiv:2306.16224 [astro-ph.HE].

[52] R. N. Manchester, G. B. Hobbs, A. Teoh, and M. Hobbs, The Australia Telescope National Facility pulsar catalogue, *Astron. J.* **129**, 1993 (2005), arXiv:astro-ph/0412641.

[53] G. Janssen *et al.*, Gravitational wave astronomy with the SKA, *PoS AASKA14*, 037 (2015), arXiv:1501.00127 [astro-ph.IM].

[54] K. Cella, S. R. Taylor, and L. Z. Kelley, Host galaxy demographics of individually detectable supermassive black-hole binaries with pulsar timing arrays, *Class. Quant. Grav.* **42**, 025021 (2025), arXiv:2407.01659 [astro-ph.GA].

[55] J. A. Ellis, A Bayesian analysis pipeline for continuous GW sources in the PTA band, *Class. Quant. Grav.* **30**, 224004 (2013), arXiv:1305.0835 [astro-ph.IM].

SUPPLEMENTARY MATERIAL

I. ANALYTIC RELATION BETWEEN PULSAR DISTANCE AND THE PULSAR-TERM INITIAL PHASE

Here we provide the explicit expression for the analytic mapping between the pulsar distance L_p and the GW parameters used in the main text. The pulsar-term initial phase Φ_p can be written as a function of the pulsar distance L_p by combining the orbital phase $\Phi_s(t)$ with the Earth–pulsar light-travel time [37]. By analytically inverting this relation with respect to L_p , we obtain

$$L_p(\Phi_p + 2k\pi, f_0, \mathcal{M}, \Phi_0) = \frac{5}{256} \frac{[1 - 16\mathcal{M}^{5/3}(\pi f_0)^{5/3}(\Phi_p + 2k\pi - \Phi_0)]^{8/5} - 1}{(1 + \hat{\Omega} \cdot \hat{p}) \mathcal{M}^{5/3}(\pi f_0)^{8/3}}, \quad (4)$$

where $k = 0, 1, 2, \dots$ accounts for the multiple solutions due to the 2π periodicity of the phase difference $(\Phi_p - \Phi_0)$, $\hat{\Omega}$ is a unit vector pointing from the GW source to the Solar System Barycenter, and \hat{p} is the unit vector pointing from the Solar System Barycenter to the pulsar.

For a given pulsar, evaluating Eq. (4) for each posterior sample yields a discrete set of distance solutions corresponding to the different k branches. These appear as a set of nearly identical peaks in the posterior for L_p . The widths of these peaks are determined by the uncertainties of the parameters entering Eq. (4). When these widths become comparable to the intrinsic spacing between the k -indexed solutions, the multi-peak structure is blurred in the marginalized posterior. In contrast, multidimensional posteriors retain more of the structure from the k -indexed solutions, as discussed in the main text.

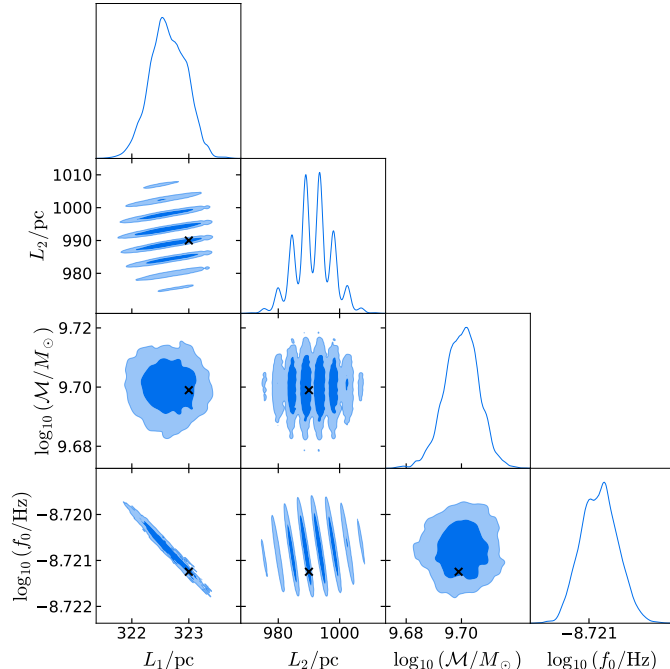


FIG. 3. Posterior distributions of \mathcal{M} , f_0 , and L_p for J0030+0451 and J0613–0200, with L_1 and L_2 representing their respective distances. Contours show the 68% and 95% credible regions. The injected true values are indicated by crosses.

II. DEGENERACIES BETWEEN PULSAR DISTANCES INDUCED BY A COMMON GRAVITATIONAL-WAVE SOURCE

Here we illustrate how degeneracies between the inferred pulsar distances arise, using a representative GW source. In Fig. 3, we show the joint posterior of the distances to pulsars J0030+0451 and J0613–0200 together with the chirp mass and initial GW frequency of an illustrative source. Each pulsar distance exhibits a clear degeneracy with the GW frequency, arising from their joint contribution to the pulsar-term phase. As a consequence, the distances to different pulsars become correlated through their shared dependence on the same GW source parameters, giving rise to a distance–distance degeneracy between L_1 and L_2 . Although the chirp mass can in principle contribute to this coupling through the phase evolution, its effect is subdominant in this example and is therefore not clearly visible in the figure. Marginalizing over the source parameters significantly suppresses the multimodality in the one-dimensional distance posteriors.

III. RESULTS FOR PULSARS AT DIFFERENT DISTANCES

Figure 4 shows that nearer pulsars can reach tighter distance constraints with fewer GW sources, whereas for more distant pulsars sub-parsec precision is achieved only in a smaller fraction of realizations even with an increased number of sources.

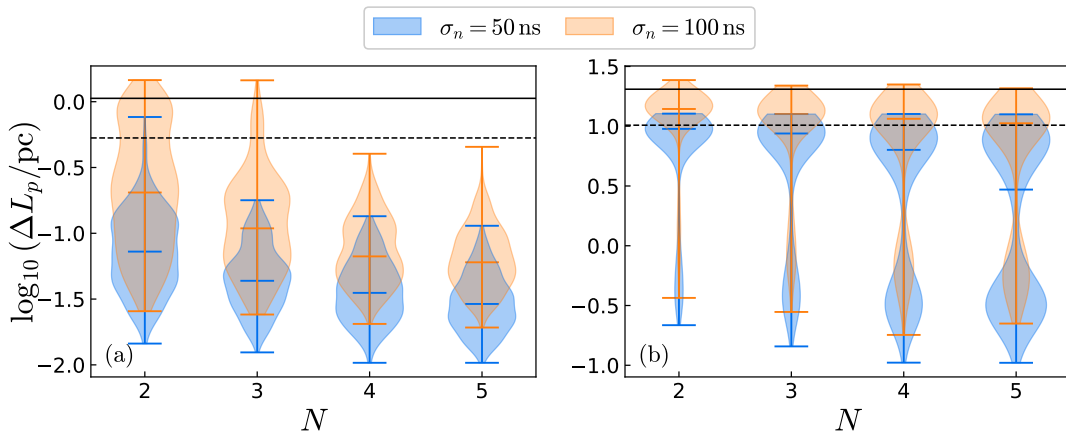


FIG. 4. Same as Fig. 2, but shown for two additional representative pulsars: (a) J0030+0451 (0.323 kpc) and (b) J1600–3053 (1.39 kpc).

IV. COMPARISON WITH ONE-DIMENSIONAL SINGLE-PULSAR DISTANCE INFERENCE

Fig. 5 compares the 2D combination and 1D combination results for a representative pulsar at 0.99 kpc (J0613–0200). The 2D combination typically yields tighter and more stable distance constraints than the 1D combination. The improvement arises from retaining the two-pulsar distance–distance structure rather than marginalizing over individual pulsar distances, enabling more efficient suppression of spurious peaks in the inferred distance distributions when combining multiple GW sources, as compared with one-dimensional single-pulsar distance inference.

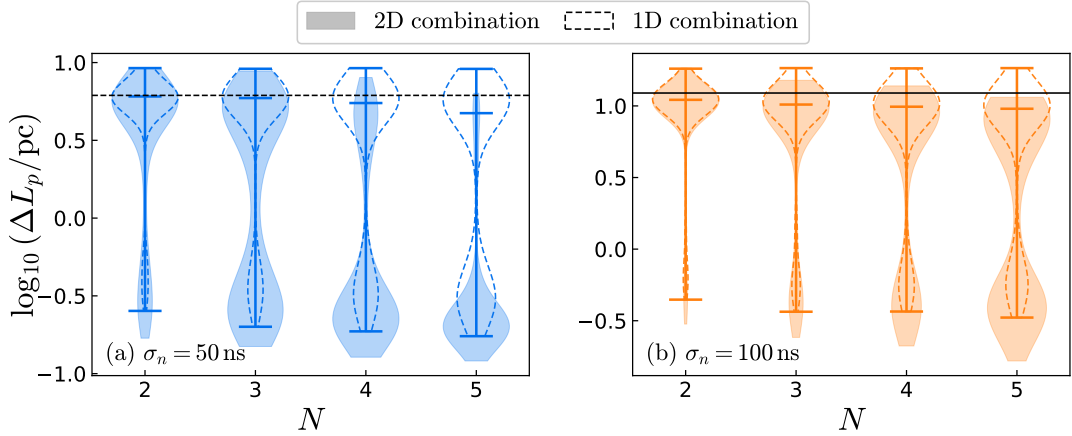


FIG. 5. Comparison between the 2D combination results and 1D combination results for pulsar-distance inference. Same as Fig. 2, shown for a representative pulsar at 0.99 kpc (J0613–0200), but with filled violins showing the 2D combination and open (dashed-outline) violins showing the 1D combination. Panels (a) and (b) correspond to $\sigma_n = 50$ ns and 100 ns, respectively.